THE JOURNAL OF NAVIGATION (2017), **70**, 184–204.
doi:10.1017/S0373463316000370

Backstepping Based Adaptive Region Tracking Fault Tolerant Control for Autonomous Underwater Vehicles

Mingjun Zhang, Xing Liu and Fei Wang

(*College of Mechanical and Electrical Engineering, Harbin Engineering University, Harbin 150001, China*)
(E-mail: liuxing20080724@gmail.com)

A region tracking fault tolerant control approach based on backstepping technique is proposed for Autonomous Underwater Vehicles (AUV). The proposed approach aims at driving tracking error to reach into the desired region in presence of ocean current disturbance, modelling uncertainty, unknown thruster faults and thruster amplitude and rate saturation constraints. At first, a type of piecewise and differential Lyapunov function is constructed to achieve region tracking control in the frame of backstepping technique. Then, the paper analyses and acquires the bound structures of the lumped uncertainty (including ocean current disturbance and model uncertainty) and the variation of thruster distribution matrix caused by unknown thruster faults, respectively. An adaptive technique is used to estimate the unknown coefficients in the above bound structures. In addition, an adaptive adjustment scheme for the desired trajectory is developed to achieve region tracking control with thruster amplitude and rate saturation constraints. The stability of the closed-loop system is analysed based on Barbalat's lemma. Finally, simulations and pool-experiments are presented to illustrate the effectiveness of the proposed method.

KEYWORDS

1. Autonomous underwater vehicle. 2. Region tracking. 3. Fault tolerant control. 4. Thruster amplitude and rate saturation constraints.

Submitted: 24 October 2015. Accepted: 26 May 2016. First published online: 4 July 2016.

1. INTRODUCTION. Autonomous Underwater Vehicles (AUVs) have been used increasingly in a variety of applications, such as long range underwater survey, exploitation of underwater resources and underwater pipeline tracking (Ataei and Yousefi-Koma, 2015; Sun et al., 2016). A trajectory tracking controller with reliability and robustness is of great importance to perform a successful mission in the unknown and complicated ocean environment (Fossen et al., 2015; Lekkas and Fossen, 2014). Therefore, it is crucial to develop a robust and reliable trajectory tracking controller for AUVs.

The main challenges in trajectory tracking control arise from the inherent nonlinearity, serious multivariate coupling and model parameter variation of an AUV subject to

external disturbance (Koofigar, 2014). In order to deal with these problems, numerous control methodologies have been proposed, including backstepping control (Bing et al., 2014; Morishita and Souza, 2014), sliding mode control (Bessa et al., 2010; Soylu et al., 2008), *H* infinity control (Slotine and Li, 1991; You et al., 2010) and artificial intelligence control (Chu et al., 2016; Seok Park, 2014). In the above cited references, the controller's goal is to acquire high tracking precision, which would result in more energy consumption. However, in some special applications, such as underwater pipeline tracking, underwater searching and plume tracking, the users pay more attention to energy consumption. In other words, they expect longer missions as long as the tracking error is within the desired region. Since the energy carried by an AUV is limited, any reductions in the energy consumption can prolong the time of AUV operation (Zhang and Chu, 2014). As for these special applications, an adaptive region tracking method was proposed for AUV based on the concept of region potential function (Li et al., 2010). Ismail and Dunnigan (2011) applied the method in tracking control of an underwater vehicle-manipulator system. On the basis of the concept of region potential function, Zhang and Chu (2014) developed an adaptive region tracking control based on Radial Basis Function (RBF) neural network and sliding mode control. Mukherjee et al. (2015) took input delay into consideration in the region tracking control. The references do not involve fault tolerant control, so these methods cannot be directly applied in cases where thruster faults occur.

During long missions in special applications, an AUV is liable to suffer from faults in the unknown and complicated ocean environment. In fact thrusters are some of the most important and common fault sources (Omerdic and Roberts, 2004). In order to accomplish fault tolerant control for an AUV with a thruster fault, Ismail et al. (2014) developed a region tracking fault tolerant control method based on weighted pseudo-inverse. Thrust reallocation is a common technique to deal with thruster faults using fault information provided by the Fault Detection and Diagnosis (FDD) module in the process of mapping the given control demand into the individual thruster forces (Johansen and Fossen; 2013, Soylu et al., 2008). The accuracy and time taken for FDD should satisfy the requirement of fault tolerant control (Jiang and Yu, 2012). Due to the features of incipient thruster fault and the ocean current disturbance, more time would be taken to acquire fault information in the FDD module, and sometimes false alarms, including missing faults, would occur. Therefore, an adaptive fault tolerant control strategy may be more suitable for cases with an incipient thruster fault. Hu et al. (2011) achieved adaptive fault tolerant control by assuming that the upper and lower bounds of an actuator fault were known in advance. Wang et al. (2012) investigated adaptive fault tolerant control based on an adaptive linear sliding mode algorithm.

The region tracking concept leads to energy saving but does not provide a solution to the problem of thruster amplitude and rate saturation constraints, especially in the initial period, due to the inevitable initial errors of the AUV. Ismail et al. (2014) adopted the joint limit concept to keep the thruster force within the saturation limits. Thrust allocation can also be used to keep the thruster force within saturation limits, such as infinity-norm based techniques (Soylu et al., 2008). These references investigated thrust amplitude saturation constraints from the view of passive adjustment and ignored thruster rate saturation constraints, but in practical applications, the thruster rate constraint has a great effect on tracking performance. In other fields, such as spacecraft, in order to tackle the actuator constraints, another strategy

has been studied using the adjustment of the desired trajectory or reference trajectory (Leonessa et al., 2009). A pseudo-control hedging scheme was proposed by modifying the reference command to prevent the adaptive element from adapting to these actuator saturations (Lombaerts et al., 2012; Simplício et al., 2013). A trajectory re-planning methodology was proposed based on differential flatness to protect the control command from violating the systems constraints (Chamseddine et al., 2013; 2015). A reference governor approach was proposed by computing a feasible reference signal to guarantee the constraints are always satisfied (Aghaei et al., 2013; Boussaid et al., 2014).

Motivated by the above considerations, region tracking fault tolerant control is investigated for AUV subject to ocean current disturbance, modelling uncertainty, unknown thruster fault and thruster amplitude and rate saturation constraints. The main contributions and novelties of the present work are presented as follows. Firstly, in the frame of backstepping technique, the paper constructs a novel types of Lyapunov functions to deal with region tracking, which is different from the concept of region potential function. In contrast to the previous results, the paper analyses the bound structures of the lumped uncertainty and the variation of the thruster distribution matrix resulting from unknown thruster faults. In order to not require the knowledge of the lumped uncertainty and thruster fault in advance, an adaptive technique is adopted to estimate the coefficients of the bounds. In addition, inspired by Leonessa et al. (2009), the paper develops a desired trajectory adjustment method to tackle thruster amplitude and rate saturation constraints by transforming these two constraints into one. Barbalat's lemma is applied to verify that the tracking errors can be reached and maintained in the designed region based on the proposed method. Finally, simulations and pool experiments are carried out to demonstrate the effectiveness of the proposed methodology.

The paper is organised as follows. Section 2 briefly describes a general model of autonomous underwater vehicles in ocean environments and formulates the control objective. Backstepping-based adaptive region tracking fault tolerant control for AUV is proposed in Section 3. Then, Section 4 studies region tracking fault tolerant control with thruster amplitude and rate saturation constraints. In Section 5, two examples are presented to illustrate the effectiveness of the proposed controller. Finally, conclusions are drawn in Section 6.

2. AUV DYNAMIC MODEL.

The nonlinear dynamic equations of AUV with six degrees of freedom in an ocean environment can be expressed as (Fossen, 2011):

$$\begin{aligned} &\dot{\eta} = J(\eta)v \\ &M\dot{v} + C_{RB}(v)v + C_A(v_r)v_r + D(v_r)v_r + g(\eta) = \tau \end{aligned} \tag{1}$$

where $J(\eta) \in R^{6\times6}$ is a spatial transformation matrix from the body fixed frame to the earth fixed frame. $\eta \in R^{6\times1}$ is the position and orientation vector of the vehicle with respect to the earth fixed frame. $v \in R^{6\times1}$ is the linear and angular velocity of the vehicle with respect to the body fixed frame. $v_r = v - v_c$. v_c is the vector of ocean current with respect to the body fixed frame. $M \in R^{6\times6}$ is the inertia matrix including added mass. $C_{RB}(v) \in R^{6\times6}$ is the rigid-body Coriolis and centripetal matrix. $C_A(v_r) \in R^{6\times6}$ is the hydrodynamic Coriolis and centripetal matrix. $D(v_r) \in R^{6\times6}$ is the drag

https://doi.org/10.1017/S0373463316000370 Published online by Cambridge University Press

matrix. $g(\eta) \in R^{6\times1}$ are the restoring forces and moments due to gravity and buoyancy. $\tau \in R^{6\times1}$ is the vector of forces and moments acting on the centroid of vehicle resulting from thrusters. The detailed expressions of these above matrixes/vectors can be seen in Podder and Sarkar (2001).

Equation (1) can be represented in the inertial fixed frame as

$$M_\eta(\eta)\ddot{\eta} + C_{RB\eta}(v,\eta)\dot{\eta} + C_{A\eta}(v_r,\eta)\dot{\eta}_r + D_\eta(v_r,\eta)\dot{\eta}_r + g_\eta(\eta) = J^{-T}\tau \tag{2}$$

where $M_\eta(\eta) = J^{-T}MJ^{-1}$, $C_{RB\eta}(v,\eta) = J^{-T}(C_{RB}\text{-}MJ^{-1}\dot{J})J^{-1}$, $C_{A\eta}(v_r,\eta) = J^{-T}C_AJ^{-1}$, $D_\eta(v_r,\eta) = J^{-T}D_AJ^{-1}$, $g_\eta(\eta) = J^{-T}g$, $\dot{\eta}_r = Jv_r$.

The control objective is to design an adaptive region tracking fault tolerant controller for AUV described as Equation (2) in order to guarantee that all the closed-loop signals are bounded and the tracking error could reach and maintain into the desired region despite being in the presence of the lumped uncertainty, unknown thruster fault and thruster amplitude and rate saturation constraints.

3. BACKSTEPPING-BASED ADAPTIVE REGION TRACKING FAULT TOLERANT CONTROL.

This section sets out to design the region tracking fault tolerant controller based on the backstepping technique. First, in order to manage tracking error to reach into the desired region, a type of piecewise and continuous function is developed to construct the Lyapunov function. Then, the paper analyses the bound structures of the lumped uncertainty and variation of thruster distribution matrix caused by thruster fault, respectively. Finally, in the frame of backstepping technique, the control law and adaptive law are derived by the constructed Lyapunov function.

3.1. *Piecewise Lyapunov function.*

The aim of a controller based on the traditional Lyapunov function is to force the tracking error to converge to zero. In order to achieve region tracking control, Li et al. (2010) proposed the concept of region potential function. Unlike the previous work, this paper investigates a region tracking controller from the view of piecewise Lyapunov function. Inspired by Wu et al. (2014), who constructed a C^n-class switching function based on power function, to avoid discontinuity caused by the breaking point in the traditional piecewise function, a type of piecewise, continuous and (n-1) order differentiable function is constructed by taking advantage of the features of exponential function and power function. The detailed expression is given as Equation (3).

$$P_{n,\varepsilon}(z) = \begin{cases} \exp(k(|z| - \varepsilon)) \times \dfrac{(|z| - \varepsilon)^n}{n!}, & |z| \geq \varepsilon \\ 0, & |z| < \varepsilon \end{cases} \tag{3}$$

where, z is variable, described in the latter; k and ε are positive constants; n is an integer and larger than one, and the detailed selection will be given later; $|z|$ denotes to take the absolute value of variable z.

As can be seen from Equation (3), $P_{n,\varepsilon}(z)$ is not less than zero. Meanwhile, according to the derivative of the generalised function (Gel'fand and Shilov, 1964), it is easy to prove the continuity and ($n-1$) order differentiable features of the constructed function. In the latter part of this paper, the piecewise Lyapunov function will be constructed based on the proposed function $P_{n,\varepsilon}(z)$.

https://doi.org/10.1017/S0373463316000370 Published online by Cambridge University Press

3.2. *Bound structure.* In the process of deriving a control law based on the constructed piecewise Lyapunov function, we should take the lumped uncertainty and unknown thruster faults into consideration. This paper deals with the effects of lumped uncertainty and thruster fault from the view of bound structure.

The considered fault is the loss of effectiveness in a thruster, which can be modelled as the variation of thruster distribution matrix B. Therefore, when thrusters are faulty, the force/torque caused by thrusters is changed from τ to τ_f.

$$\tau_f = Bu - BKu = (B + \tilde{B})u \tag{4}$$

where, u is the control input of thrusters. K is a diagonal matrix, and its diagonal element $k_{\mathrm{ii}} \in [0,1]$; $k_{ii} = 0$ denotes the ith thruster is healthy; $k_{ii} = 1$ denotes the ith thruster is failing; $k_{ii} \in (0,1)$ denotes the ith thruster has a partial loss fault.

Due to the property of K, namely $\|K\| < 1$, it can be derived from $\left\|\tilde{B}B^{+}\right\| < \|K\|\|BB^{+}\|$. Hence, there exists an unknown constant $L \in (0, 1)$, so the following inequality holds

$$\left\|\tilde{B}B^{+}\right\| < L \tag{5}$$

where, B^{+}denotes the pseudo-inverse of matrix B, and $\|\|$ denotes Euclidean norm.

Due to the inherent nonlinearity and serious multivariate coupling, an AUV dynamic model based on the dynamic modelling technique has great uncertainty (Zhang et al., 2015). In this paper, the modelling uncertainty is expressed as follows:

$$\begin{aligned} M_\eta &= \hat{M}_\eta + \tilde{M}_\eta;\ C_{RB\eta} = \hat{C}_{RB\eta} + C_{RB\eta};\ C_{A\eta} = \hat{C}_{A\eta} + \tilde{C}_{A\eta};\ D_\eta = \hat{D}_\eta + \tilde{D}_\eta; \\ g_\eta &= \hat{g}_\eta + \tilde{g}_\eta \end{aligned} \tag{6}$$

According to the analysis presented above, the model of an AUV with lumped uncertainty and thruster fault can be described as

$$\ddot{\eta} = \hat{M}_\eta^{-1}\left[J^{-T}(B + \tilde{B})u - \hat{C}_{RB\eta}\dot{\eta} - \hat{C}_{A\eta}\dot{\eta} - \hat{D}_\eta\dot{\eta} - \hat{g}_\eta\right] - H \tag{7}$$

where, $H = \hat{M}_\eta^{-1}(\tilde{M}_\eta\ddot{\eta} + \tilde{C}_{RB\eta}\dot{\eta} + \tilde{C}_{A\eta}\dot{\eta}_r - C_{A\eta}Jv_c + \tilde{D}_\eta\dot{\eta}_r - D_\eta Jv_c + \tilde{g}_\eta)$.

In general, the amplitude of ocean current is bounded. From the structure of the AUV dynamic model in Podder and Sarkar (2001), it has the following inequalities:

$$\begin{aligned} &\left\|\hat{M}_\eta^{-1}\tilde{M}_\eta\ddot{\eta}\right\| < b_0 + b_1\|\dot{\eta}\| + b_2\|\dot{\eta}\|^2;\ \left\|\hat{M}_\eta^{-1}\tilde{C}_{RB\eta}\dot{\eta}\right\| < c_0\|\dot{\eta}\|^2; \\ &\left\|\hat{M}_\eta^{-1}\tilde{C}_{A\eta}\dot{\eta}_r\right\| = \left\|\hat{M}_\eta^{-1}\tilde{C}_{A\eta}(\dot{\eta} - Jv_c)\right\| < c_1\|\dot{\eta}\|^2 + c_2\|\dot{\eta}\|; \\ &\left\|\hat{M}_\eta^{-1}C_{A\eta}Jv_c\right\| < c_3\|\dot{\eta}\|;\ \left\|\hat{M}_\eta^{-1}\tilde{D}_\eta(\dot{\eta} - Jv_c)\right\| < d_0\|\dot{\eta}\|^2 + d_1\|\dot{\eta}\|; \\ &\left\|\hat{M}_\eta^{-1}D_\eta Jv_c\right\| < d_2\|\dot{\eta}\|;\ \left\|\hat{M}_\eta^{-1}\tilde{g}_\eta\right\| < d_3 \end{aligned}$$

where b_i, c_i, d_i $(i = 0,1,2,3)$ are all positive constants.

https://doi.org/10.1017/S0373463316000370 Published online by Cambridge University Press

Consequently, according to the structure of inequalities presented above, it can be concluded that there exist unknown and constant vectors $\varphi_i > 0$, $i = 0,1,2$, so the following inequality holds

$$\|H\| < \varphi_0 + \varphi_1\|\dot{\eta}\| + \varphi_2\|\dot{\eta}\|^2 \tag{8}$$

3.3. *Control law formulation.* According to the above-presented piecewise Lyapunov function Equation (3), the bound structures of the variation of thruster distribution matrix caused by thruster fault Equation (5), and the bound structure of the lumped uncertainty Equation (8), this paper derives the control law.

At first, the desired trajectory is transferred as a reference trajectory, so as to acquire the position/orientation, velocity and acceleration of the reference trajectory which are required to construct the controller. The following second-order system is adopted as the trajectory reference model, given by

$$\begin{pmatrix} \dot{\eta}_R \\ \ddot{\eta}_R \end{pmatrix} = \begin{pmatrix} 0_{6\times6} & I_{6\times6} \\ -\omega_n^2 I_{6\times6} & -2\omega_n\xi I_{6\times6} \end{pmatrix} \begin{pmatrix} \eta_R \\ \dot{\eta}_R \end{pmatrix} + \begin{pmatrix} 0_{6\times6} \\ \omega_n^2 I_{6\times6} \end{pmatrix} \eta_d \tag{9}$$

where, $\eta_d \in R^{6\times1}$ is the desired trajectory, $\eta_R \in R^{6\times1}$ is the reference state vector. ω_n and ξ are positive constants.

Before designing the adaptive region tracking fault tolerant controller based on the backstepping technique, we define the following variables z_1 and z_2

$$\begin{aligned} z_1 &= \eta - \eta_R \\ z_2 &= \dot{\eta} - \alpha \end{aligned} \tag{10}$$

where, α is the virtual variable and will be designed later.

According to the above-presented piecewise function Equation (3), we define a Lyapunov function in terms of tracking error z_1

$$V_1 = \sum_{i=1}^{6} P_{3,\varepsilon_1(i)}(z_1(i)) \tag{11}$$

where, ε_1 is the desired tracking error region; $\varepsilon_1(i)$ is the ith element of vector ε_1; $z_1(i)$ is the ith element of vector z_1; $V_1 \geq 0$.

The time derivative of Equation (11) is presented as follows:

$$\dot{V}_1 = \sum_{i=1}^{6} (kP_{3,\varepsilon_1(i)}(z_1(i)) + P_{2,\varepsilon_1(i)}(z_1(i)))sign(z_1(i))\dot{z}_1(i) \tag{12}$$

Apparently, discontinuity may exist in the latter derivative due to the sign function in Equation (12). However, after further analysing the property of function as Equation (3), it can be found that sign(z_1) could not affect the continuity of V_1, since function $P_{3,\varepsilon_1}(i)(z_1(i))$ equals zero in the interval of $[-\varepsilon_1(i), \varepsilon_1(i)]$, but it would affect the continuity of the virtual variable α and control law. Based on the fact that the value of sign(z_1) on the interval of $[-\varepsilon_1(i), \varepsilon_1(i)]$ does not change the value of $\dot{V}_1$, another sign-like function takes the place of sign(z_1) in this paper, shown as Equation (13) so as to not introduce the sign(z_1) in the latter control law. Specifically, in the interval of $[-\varepsilon_1(i), \varepsilon_1(i)]$, trigonometric functions are adopted to avoid the breaking point in the traditional sign

https://doi.org/10.1017/S0373463316000370 Published online by Cambridge University Press

function.

$$\mathrm{sgn}_{\varepsilon_1(i)}(z_1(i)) = \begin{cases} sign(z_1(i)), & |z_1| \geq \varepsilon_1(i) \\ \sin\left(\frac{\pi}{2}\cos\left(\frac{\pi}{2}\frac{z_1(i)-\varepsilon_1(i)}{\varepsilon_1(i)}\right)\right), & |z_1| < \varepsilon_1(i) \end{cases} \tag{13}$$

where, $\mathrm{sgn}_{\varepsilon_1(i)}(z_1(i))$ is continuous and the derivative can be calculated by treating it as generalised function.

Using Equations (10) and (13), Equation (12) can be represented by vector form as Equation (14)

$$\dot{V}_1 = \Sigma(kP_{3,\varepsilon_1}(z_1) + P_{2,\varepsilon_1}(z_1))\mathrm{sgn}_{\varepsilon_1}(z_1)(z_2 + \alpha - \dot{\eta}_R) \tag{14}$$

where, $P_{3,\varepsilon_1}(z_1) = [P_{3,\varepsilon_1(1)}(z_1(1)), P_{3,\varepsilon_1(2)}(z_1(2)), \cdots, P_{3,\varepsilon_1(6)}(z_1(6))]^T$; vector $\mathrm{sgn}_{\varepsilon_1}(z_1)$ and $P_{2,\varepsilon_1}(z_1)$ are similar as $P_{3,\varepsilon_1}(z_1)$. ΣX denotes to calculate the sum of all elements in vector X. We note that the product of vectors with the same dimensions should be operated as a product of the corresponding elements in the vectors. For example, the product of $[x_1,x_2,x_3]^T$ and $[y_1,y_2,y_3]^T$ is $[x_1y_1, x_2y_2, x_3y_3]^T$.

We design the virtual variable α

$$\alpha = -\left(g_1 + \frac{1}{4}\right)(kP_{3,\varepsilon_1}(z_1) + P_{2,\varepsilon_1}(z_1))\mathrm{sgn}_{\varepsilon_1}(z_1) + \dot{\eta}_R - (\varepsilon_2 + \sigma)\mathrm{sgn}_{\varepsilon_1}(z_1) \tag{15}$$

where, g_1 is positive constant; σ is positive vector. It can be simply verified that the virtual variable α is continuous and differentiable based on the generalised function.

Next, according to the above-presented function, we define a Lyapunov function in terms of the variable z_2

$$V_2 = V_1 + \Sigma P_{2,\varepsilon_2}(z_2) \tag{16}$$

The time derivative of V_2 is

$$\dot{V}_2 = \dot{V}_1 + \Sigma(kP_{2,\varepsilon_2}(z_2) + P_{1,\varepsilon_2}(z_2))\mathrm{sgn}_{\varepsilon_2}(z_2)(\ddot{\eta} - \dot{\alpha}) \tag{17}$$

Substituting Equation (7) into Equation (17), yields

$$\begin{aligned} \dot{V}_2 = {} & \dot{V}_1 + \Sigma(kP_{2,\varepsilon_2}(z_2) + P_{1,\varepsilon_2}(z_2))\mathrm{sgn}_{\varepsilon_2}(z_2) \\ & \left(\hat{M}_\eta^{-1}\left[J^{-T}(B + \tilde{B})u - \dot{\eta} - \hat{C}_{A\eta}\dot{\eta} - \hat{D}_\eta\dot{\eta} - \hat{g}_\eta\right] - H - \dot{\alpha}\right) \end{aligned} \tag{18}$$

The first main result of this paper is given in the following.

Theorem 1: Consider an AUV described as in Equation (7) subject to the lumped uncertainty and unknown thruster faults, all the closed-loop signals are bounded and the tracking error could reach into the desired region with the action of the control law, expressed as Equations (19a)–(19c) and adaptive law, expressed as

https://doi.org/10.1017/S0373463316000370 Published online by Cambridge University Press

Equations (20a)–(20d).

$$\begin{aligned} u = B^{+}J^{T}[(\hat{C}_{RB\eta}\dot{\eta} + \hat{C}_{A\eta}\dot{\eta} + \hat{D}_{\eta}\dot{\eta} + \hat{g}_{\eta}) + \hat{M}_{\eta}\dot{\alpha}_1 \\ - (g_2+1)\hat{M}_{\eta}P_{1,\varepsilon_2}(z_2)\mathrm{sgn}_{\varepsilon 2}(z_2)] + u_1 + u_2 \end{aligned} \tag{19a}$$

$$u_1 = -B^{+}J^{T}\hat{M}_{\eta}(\hat{\rho}_0 + \hat{\rho}_1\|\dot{\eta}\| + \hat{\rho}_2\|\dot{\eta}\|^2)\mathrm{sgn}_{\varepsilon_2}(z_2) \tag{19b}$$

$$\begin{aligned} u_2 = -B^{+}J^{T}\hat{\rho}_3\|[(\hat{C}_{RB\eta}\dot{\eta} + \hat{C}_{A\eta}\dot{\eta} + \hat{D}_{\eta}\dot{\eta} + \hat{g}_{\eta}) + \hat{M}_{\eta}\dot{\alpha}_1 \\ - (g_2+1)\hat{M}_{\eta}P_{1,\varepsilon_2}(z_2)\mathrm{sgn}_{\varepsilon_2}(z_2)]\|\mathrm{sgn}_{\varepsilon_2}(z_2) \end{aligned} \tag{19c}$$

$$\dot{\hat{\rho}}_0 = \Gamma_0(kP_{2,\varepsilon_2}(z_2) + P_{1,\varepsilon_2}(z_2)) \tag{20a}$$

$$\dot{\hat{\rho}}_1 = \Gamma_1(kP_{2,\varepsilon_2}(z_2) + P_{1,\varepsilon_2}(z_2))\|\dot{\eta}\| \tag{20b}$$

$$\dot{\hat{\rho}}_2 = \Gamma_2(kP_{2,\varepsilon_2}(z_2) + P_{1,\varepsilon_2}(z_2))\|\dot{\eta}\|^2 \tag{20c}$$

$$\begin{aligned} \dot{\hat{\rho}}_3 = \Gamma_3\hat{M}_{\eta}^{-1}(kP_{2,\varepsilon_2}(z_2) + P_{1,\varepsilon_2}(z_2)) \\ \left\|[(\hat{C}_{RB\eta}\dot{\eta} + \hat{C}_{A\eta}\dot{\eta} + \hat{D}_{\eta}\dot{\eta} + \hat{g}_{\eta}) + \hat{M}_{\eta}\dot{\alpha}_1 - (g_2+1)\hat{M}_{\eta}P_{1,\varepsilon_2}(z_2)\mathrm{sgn}_{\varepsilon_2}(z_2)]\right\| \end{aligned} \tag{20d}$$

where, g_2 is positive constant; $\rho_i = \varphi_i/(1-L)$ $i = 0,1,2.$; $\hat{\rho}_k$ is the estimation of ρ_k, $k = 0,1,2,3$. $\rho_3 = [L/(1-L), L/(1-L), L/(1-L)]^T$; Γ_j ($j = 0,1,2,3$) are diagonal and positive definite matrix.

The proof of *Theorem 1* is given in Appendix A.

From the derivation and analysis procedure presented above, the proposed region tracking fault tolerant control algorithm is robust to ocean current disturbance and model uncertainty due to its adaptive term. It could also compensate unknown thruster faults, independent of the FDD.

4. REGION TRACKING FAULT TOLERANT CONTROL WITH THRUSTER AMPLITUDE AND RATE SATURATION CONSTRAINTS.

This section extends the proposed region tracking fault tolerant controller described in Section 3 to region tracking fault tolerant control with thruster amplitude and rate saturation constraints.

With respect to control input constraints, the strategies based on adjustment of the desired trajectory have been investigated in recent years, including pseudo-control hedging, trajectory re-planning and reference governors. In contrast to the technique in Leonessa et al. (2009), which was accomplished in the respect of the derivative of control law, we investigate thruster amplitude and rate saturation constraints based on thruster constraints transfer and the relationship between the controller output and the desired trajectory.

4.1. *Constraints Transfer.*

At first, the thruster amplitude and rate saturation constraints can be described as

$$\begin{aligned} u_{\min} \le u \le u_{\max} \\ \gamma_{\min} \le \dot{u} \le \gamma_{\max} \end{aligned} \tag{21}$$

where, $u_{\max}$ and $u_{\min}$ are the upper and lower limits of thruster amplitude. $\gamma_{\max}$ and $\gamma_{\min}$ are the upper and lower limits of thruster rate.

https://doi.org/10.1017/S0373463316000370 Published online by Cambridge University Press

Thruster amplitude and rate saturation constraints can be transferred to a single constraint, namely Equation (21) can be approximately transformed as

$$\underline{u} \le u \le \bar{u} \tag{22}$$

where, $\underline{u} = \max\{u_{\min} \quad u(t-T) + T\gamma_{\min}\}$; $\bar{u} = \min\{u_{\max} \quad u(t-T) + T\gamma_{\max}\}$; Equation (22) can be derived based on the approximation relationship $\dot{u} \approx (u(t) - u(t-T))/T$. $u(t)$ and $u(t-T)$ are the present and previous step of thruster output, respectively. T is the control interval.

4.2. *Desired trajectory adjustment.* Recalling the control law in Equation (19a) and Equation (15), the controller output $\boldsymbol{u}$ explicitly depends on the desired trajectory.

Using Equations (9), (15) and (19a)–(19c), the desired trajectory can be expressed as

$$\begin{aligned}\eta_d = (w_n^2 J^T \hat{M}_\eta)^{-1} B(u - B^+ J^T[(\hat{C}_{RB\eta}\dot{\eta} + \hat{C}_{A\eta}\dot{\eta} + \hat{D}_\eta\dot{\eta} + \hat{g}_\eta) \\ + \hat{M}_\eta\left(\frac{df(z_1)}{dt} - \omega_n^2\eta_R - 2\omega_n\xi\dot{\eta}_R\right) - (g_2+1)\hat{M}_\eta P_{1,\varepsilon_2}(z_2)\mathrm{sgn}_{\varepsilon_2}(z_2)] + u_1 + u_2)\end{aligned} \tag{23}$$

where, $f(z_1) = -(g_1 + \frac{1}{4})(kP_{3,\varepsilon_1}(z_1) + P_{2,\varepsilon_1}(z_1))\mathrm{sgn}_{\varepsilon_1}(z_1) - (\varepsilon_2 + \sigma)\mathrm{sgn}_{\varepsilon_1}(z_1)$.

To deal with thruster amplitude and rate saturation constraints, the desired trajectory should be shaped to guarantee the control output $\boldsymbol{u}$ in Equation (23) to satisfy Equation (22).

Next, another important result is presented:

Theorem 2: Consider an AUV described as per Equation (1) with the lumped uncertainty, unknown thruster fault and thruster amplitude and rate saturation constraints, control laws designed as Equations (19a)–(19c) and adaptive laws expressed as Equations (20a)–(20d). The desired trajectory is modified as follows

$$\eta_d' = \eta_d + (\omega_n^2 J^T \hat{M}_\eta)^{-1} B u^*(\delta(u^*) - 1) \tag{24}$$

where, $\delta(u^*) = \begin{cases} \bar{u}/u^* & u^* > \bar{u} \\ 1 & \underline{u} \le u^* \le \bar{u} \\ \underline{u}/u^* & u^* < \underline{u} \end{cases}$; u^* is the control output without considering thruster constraints in Section 3. Then, the following statements hold:

(i) The tracking error could be reached in the designed region ε_1;
(ii) The control output would satisfy Equation (22).

The proof of *Theorem 2* is given in Appendix B.

From the above design and analysis, it can be concluded that the proposed method could deal with thruster amplitude and rate saturation constraints by locally modifying the desired trajectory. Thus we have tracking fault tolerant control for an AUV with lumped uncertainty, unknown thruster faults and thruster amplitude and rate saturation constraints.

5. SIMULATIONS AND POOL EXPERIMENTS.

In this section, simulation and experiment results are presented to demonstrate the feasibility and effectiveness

https://doi.org/10.1017/S0373463316000370 Published online by Cambridge University Press

of the proposed method. For this purpose, two examples are considered. In the first example, a series of simulations of an *ODIN* AUV are performed. In the second example, the proposed region tracking fault tolerant controller is used to experiment on *Beaver 2* AUV, designed by the authors' laboratory.

5.1. *Simulations on ODIN AUV.* In order to verify the effectiveness of the proposed region tracking fault tolerant controller, a serial of simulations were conducted on an *ODIN* AUV subject to ocean current disturbance, modelling uncertainty, unknown thruster fault, and thruster amplitude and rate saturation constraints. The parameters of the *ODIN* AUV can be seen in Podder and Sarkar (2001). The thruster distribution matrix in the considered *ODIN* AUV is expressed as follows.

$$B = \begin{bmatrix} s & -s & -s & s & 0 & 0 & 0 & 0 \\ s & s & -s & -s & 0 & 0 & 0 & 0 \\ 0 & 0 & 0 & 0 & -1 & -1 & -1 & -1 \\ 0 & 0 & 0 & 0 & Rs & Rs & -Rs & -Rs \\ 0 & 0 & 0 & 0 & Rs & -Rs & -Rs & Rs \\ R_z & -R_z & R_z & -R_z & 0 & 0 & 0 & 0 \end{bmatrix}$$

where $s = \sin(\text{pi}/4)$; $R = 0{\cdot}381$; $R_z = 0{\cdot}508$.

In this section, 30% model uncertainty is set for each of the parameters in the *ODIN* AUV, which means the nominal system dynamics used in the controller is 70%. The ocean current speed V_c is generated using a first-order Gauss-Markov process, expressed as Equation (25) (Fossen, 2011).

$$\dot{V}_c + \mu V_c = \omega \tag{25}$$

where ω is Gaussian white noise with mean $-1{\cdot}5$ and variance 1; $\mu = 3$; two angles concerning the direction of ocean current: β_c (sideslip angle) and α_c (angle of attack); β_c is generated by the sum of Gaussian noise with mean 0 and variance 50; and $\alpha_c = \beta_c/2$.

There are two kinds of incipient thruster faults considered in this paper, shown as Equations (26) and (27).

$$k_{11} = \begin{cases} 0, & t < 20 \\ \dfrac{0{\cdot}29}{30}(t-20) + 0{\cdot}01\sin\left(\dfrac{\pi}{5}(t-20)\right), & 20 \le t < 50 \\ \dfrac{0{\cdot}29}{30} + 0{\cdot}01\sin\left(\dfrac{\pi}{10}(t-50)\right), & t \ge 50 \end{cases} \tag{26}$$

$$k_{11} = \begin{cases} 0, & t < 20 \\ 0{\cdot}5\left(1 - \exp\left(\dfrac{-(t-20)}{10}\right)\right), & t \ge 50 \end{cases} \tag{27}$$

The initial position of the *ODIN* AUV is $\eta_0 = [0{\cdot}4;\ 0{\cdot}4;-0{\cdot}4;\ \text{pi}/18;\ \text{pi}/18;\ \text{pi}/9]$ and its initial velocity is zero. Furthermore, it is assumed that the thruster amplitude limits are ±200N, and the thruster rate limits are ±100N/s, namely, $u_{\max} = 200$; $u_{\min} = -200$; $\gamma_{\max} = 100$ and $\gamma_{\min} = -100$.

https://doi.org/10.1017/S0373463316000370 Published online by Cambridge University Press

The parameters in the proposed method in Section 3 are given as follows:

$$\varepsilon_1 = [0{\cdot}3, 0{\cdot}3, 0{\cdot}3, 0{\cdot}15, 0{\cdot}15, 0{\cdot}15]'; \varepsilon_2 = [0{\cdot}5, 0{\cdot}5, 0{\cdot}5, 0{\cdot}25, 0{\cdot}25, 0{\cdot}25]';$$

$$g_1 = 2; g_2 = 5; k = 1; w_n = 3; \xi = 0{\cdot}7; \sigma = [0{\cdot}1, 0{\cdot}1, 0{\cdot}1, 0{\cdot}1, 0{\cdot}1, 0{\cdot}1]';$$

$$\boldsymbol{\Gamma_0} = \mathrm{diag}(0{\cdot}5; 0{\cdot}5; 0{\cdot}5; 0{\cdot}05; 0{\cdot}05; 0{\cdot}05);$$

$$\boldsymbol{\Gamma_1} = \mathrm{diag}(0{\cdot}5; 0{\cdot}5; 0{\cdot}5; 0{\cdot}05; 0{\cdot}05; 0{\cdot}05);$$

$$\boldsymbol{\Gamma_2} = \mathrm{diag}(0{\cdot}5; 0{\cdot}5; 0{\cdot}5; 0{\cdot}05; 0{\cdot}05; 0{\cdot}05);$$

$$\boldsymbol{\Gamma_3} = \mathrm{diag}(0{\cdot}5; 0{\cdot}5; 0{\cdot}5; 0{\cdot}05; 0{\cdot}05; 0{\cdot}05);$$

Now, the proposed method is used to track two kinds of trajectories: an ellipse shape and a figure of eight curve shape.

5.1.1. *An ellipse shape trajectory.* The ellipse shape desired trajectory is given by

$$x_d = 6(1 - \cos(0{\cdot}15t)); y_d = 3\sin(0{\cdot}15t); z_d = -0{\cdot}2x_d; \eta_d = [x_d, y_d, z_d, 0, 0, 0]$$

The following three cases are considered.

Case 1: No thruster fault occurs;

Case 2: The first thruster fault occurs as Equation (26); and the fifth thruster completely fails after the 20th second;

Case 3: The first thruster fault occurs as Equation (27); and the fifth thruster completely fails after the 20th second.

Figures 1 and 2 illustrate the simulation results about path, tracking error and control output for Case 1, Case 2 and Case 3, respectively.

As can be seen from Figures 1 and 2, no matter whether thruster faults occur, the tracking error could be reached and maintained into the desired region based on the developed region tracking controller, while tracking the ellipse shape trajectory. Moreover, in these cases, affected by the thruster rate saturation constraint, the control outputs do not change abruptly in the initial period, although there exists the initial error. The control outputs do not violate the thruster constraints in the whole process.

5.1.2. *Figure of eight curve shape trajectory.* In a similar way, a different desired trajectory is considered in the paper, given by

$$x_d = 4(1 - \cos(0{\cdot}10t)); y_d = 2\sin(0{\cdot}20t); z_d = -0{\cdot}2x_d; \eta_d = [x_d, y_d, z_d, 0, 0, 0]$$

In this subsection, simulation is carried out in the condition of Case 2. The simulation result is shown in Figure 3.

As shown in Figure 3, although the tracking error is outside of the desired region in the initial period, after about 10 seconds, the tracking error could be in the desired region based on the proposed region tracking controller, even after thruster faults have occurred.

In addition, in order to further demonstrate the effectiveness of the proposed method, the simulations with another new desired region (ε_1) are performed. The new desired region is set as ε_1 = [0·1,0·1,0·05,0·05,0·05]', and the other parameters are the same as those in Case 2.

Figure 4 shows the tracking errors for the two tracking cases. According to Figure 4, the tracking errors could be reached and maintained in the new desired region after about 5 seconds. The simulation results are tabulated in Tables 1 and 2.

https://doi.org/10.1017/S0373463316000370 Published online by Cambridge University Press

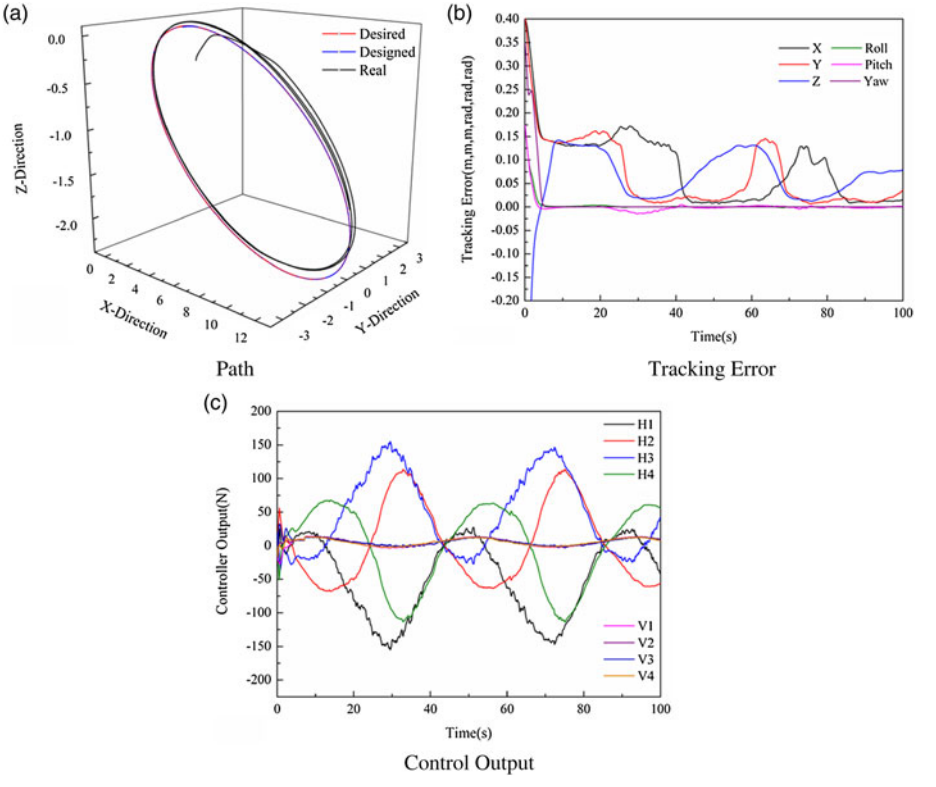

Figure 1. Simulation results for Case 1 of the ellipse shape trajectory.

5.1.3. *Comparative simulation studies.* In order to demonstrate the efficacy of the proposed region tracking method, comparative simulation studies were performed based on the concept of region potential function. The comparative simulations are divided into two parts, that is, one is the case without ocean current disturbance, and the other is the case with ocean current disturbance after the 50th second simulated as Equation (25). In the comparative simulations, the desired region $\varepsilon_1 = [0{\cdot}3,0{\cdot}3,0{\cdot}3,0{\cdot}15,0{\cdot}15,0{\cdot}15]'$. The initial position and orientation $\eta_0 =$ [0·04;0·04;–0·04; pi/360;pi/360;pi/180]'. The controller parameters $K_p = 500$*diag (5,5,5,3,3,3); $L_d = 20I_{13\times13}$; $K_v =$ diag(500,500,500,30,30,30). The detailed controller expression was given in Ismail et al. (2014).

Figure 5 shows the tracking errors for tracking the ellipse shape trajectory with/without ocean current disturbance while Figure 6 shows the results of tracking another trajectory.

From Figures 5 and 6, in the case of no ocean current disturbance, the tracking errors could be maintained in the desired regions for the two desired trajectories. This indicates that the concept of region potential function can be adopted to achieve region tracking control without external disturbance. However, in the presence of ocean current disturbance, the tracking errors obtained from the comparative method are out of the desired region. Therefore, in comparison with the concept of

https://doi.org/10.1017/S0373463316000370 Published online by Cambridge University Press

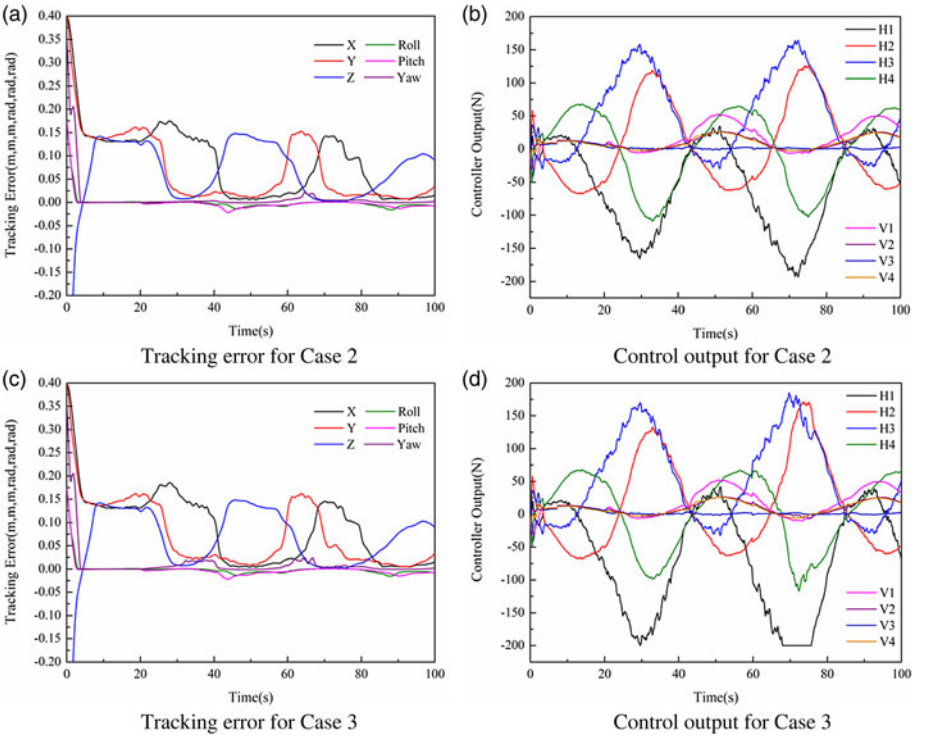

Figure 2. Simulation results for Case 2 and Case 3 of the ellipse shape trajectory.

region potential function, the simulation results demonstrate the efficacy of the proposed region tracking method.

5.2. *Experiments on Beaver 2 AUV.* Another example is considered in the paper to verify the efficacy of the proposed method. In the example, experiments are performed on the *Beaver 2* AUV, designed by the authors' laboratory in 2014 (thrusters were changed in 2015), shown in Figure 7(a). The *Beaver 2* AUV was 0·8 m × 0·5 m × 0·4 m. Its dry weight was 50 kg and slightly positively buoyant. The left and right thrusters were configured in *Beaver 2*, which can provide a maximum thrust of approximately 30N. Figure 7(b) describes the hardware architecture of *Beaver 2*.

It should be explained that in order to conduct experiments conveniently, the power of *Beaver 2* comes from outside by the umbilical cable, but the controller algorithm runs in the PC104 working with *Vxworks* embedded control system inside *Beaver 2*. The host computer is in charge of sending only Start/Stop commands and receiving and saving experiment data. The sensor system was composed of HMR3000 digital compass (measuring roll, pitch and yaw angles), and Mini-Avatar (measuring angular velocities).

In this section, the yaw angle tracking is considered. The yaw model of *Beaver 2* used to synthesize controller is described as follows (Zhang et al., 2015).

$$M_\psi \dot{r} + D_{\psi 1} r + D_{\psi 2} r|r| + g_\psi = T_r \tag{28}$$

https://doi.org/10.1017/S0373463316000370 Published online by Cambridge University Press

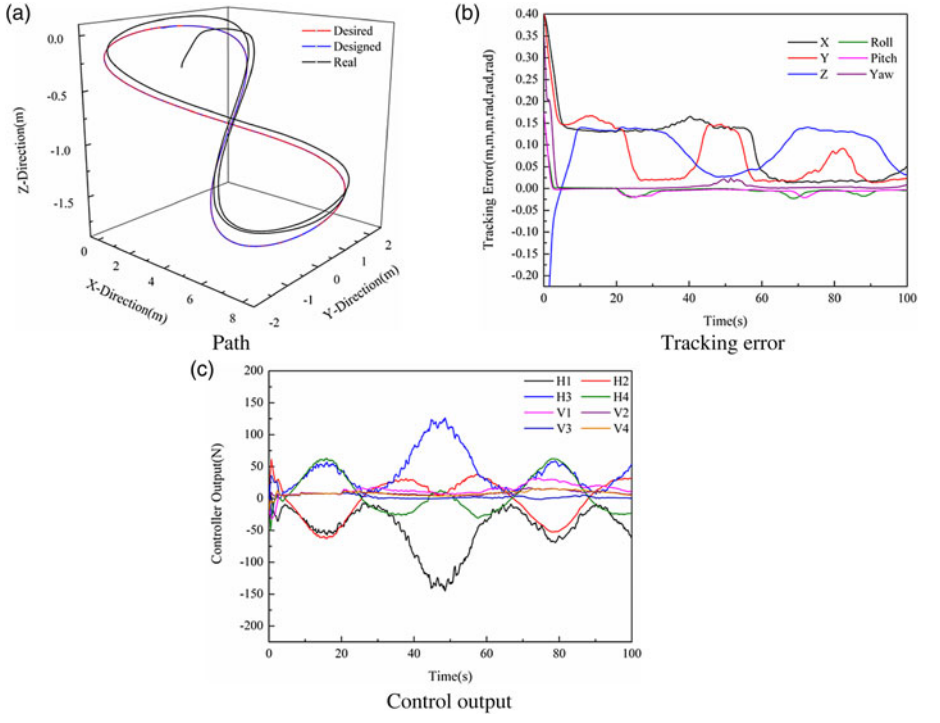

Figure 3. Simulation results of the figure of eight curve shape trajectory.

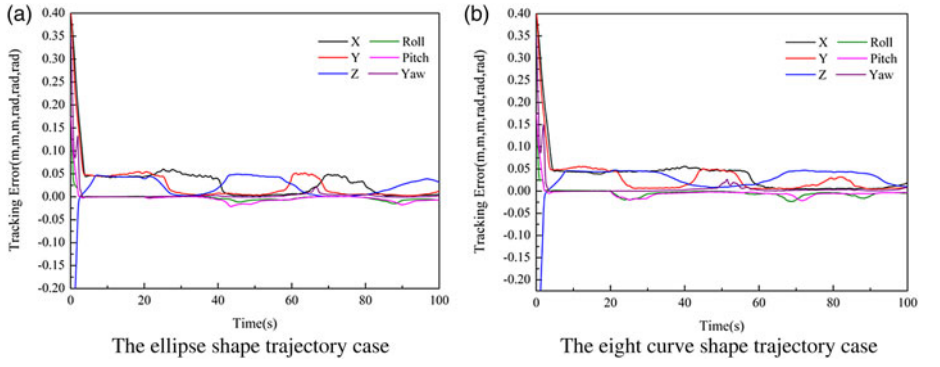

Figure 4. Simulation results for another desired region.

where $M_\psi = 22{\cdot}0753$; $D_{\psi 1} = 4{\cdot}4458$; $D_{\psi 2} = 15{\cdot}4308$; $g_\psi = 0{\cdot}5828$; T_r is the torque generated by thrusters.

In the experiments, two desired yaw angles are considered, shown as follows.

$$\psi_{d1} = 0{\cdot}75\pi(1 - \exp(-0{\cdot}1t)) \tag{29}$$

$$\psi_{d2} = \begin{cases} 0{\cdot}45\pi(1 - \exp(-0{\cdot}1t)) & 0 \le t \le 50 \\ 0{\cdot}45\pi + 0{\cdot}3\pi(1 - \exp(-0{\cdot}1(t - 50))) & 50 < t \end{cases} \tag{30}$$

https://doi.org/10.1017/S0373463316000370 Published online by Cambridge University Press

Table 1. Region tracking performance of the ellipse shape trajectory after 10 seconds.

		Position Error (m)			Orientation Error (rad)		
		X	Y	Z	Pitch	Roll	Yaw
Case 1	Desired Region	0·30	0·30	0·30	0·15	0·15	0·15
	Maximum Error	0·17	0·16	0·14	0·0036	0·0047	1·5E-06
Case 2	Desired Region	0·30	0·30	0·30	0·15	0·15	0·15
	Maximum Error	0·17	0·16	0·15	0·0010	0·0012	0·023
Case 3	Desired Region	0·30	0·30	0·30	0·15	0·15	0·15
	Maximum Error	0·19	0·16	0·15	0·0010	0·0014	0·024
Case 2	Desired Region	0·10	0·10	0·10	0·05	0·05	0·05
	Maximum Error	0·060	0·055	0·049	0·0009	0·0010	0·021

Table 2. Region tracking performance of the figure of eight curve shape trajectory after 10 seconds.

		Position Error (m)			Orientation Error (rad)		
		X	Y	Z	Pitch	Roll	Yaw
Case 2	Desired Region	0·30	0·30	0·30	0·15	0·15	0·15
	Maximum Error	0·17	0·17	0·14	0·001	0·00006	0·024
Case 2	Desired Region	0·10	0·10	0·10	0·05	0·05	0·05
	Maximum Error	0·056	0·056	0·047	0·001	9·7E-05	0·027

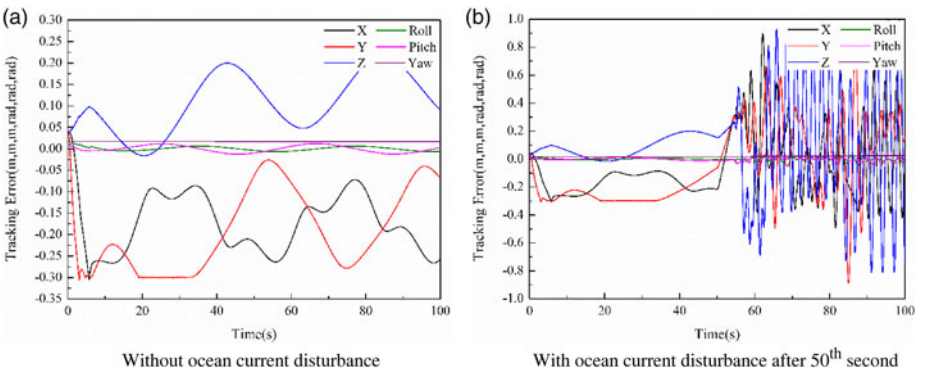

Figure 5. Comparative simulation results for the ellipse shape trajectory.

Similar to Section 5.1, two kinds of thruster faults are taken into account in the experiments. The expressions of thruster faults are the same as Equations (26) and (27). The thruster distribution matrix is expressed as $B = [-0{\cdot}74, 0{\cdot}74]$.

The parameters in the controller are given in the following:

$$\varepsilon_1 = 0{\cdot}1; \varepsilon_2 = 0{\cdot}3; c_1 = 2; c_2 = 5; k = 1; w_n = 3; \xi = 0{\cdot}7;$$
$$\sigma = 0{\cdot}1;\ \Gamma_0 = 0{\cdot}001;\ \Gamma_1 = 0{\cdot}001;\ \Gamma_2 = 0{\cdot}001;\ \Gamma_3 = 0{\cdot}005;$$

Figures 8 and 9 illustrate the tracking errors for the above desired yaw angles, when the two kinds of faults occur in the first thruster, respectively. As can be seen from Figures

https://doi.org/10.1017/S0373463316000370 Published online by Cambridge University Press

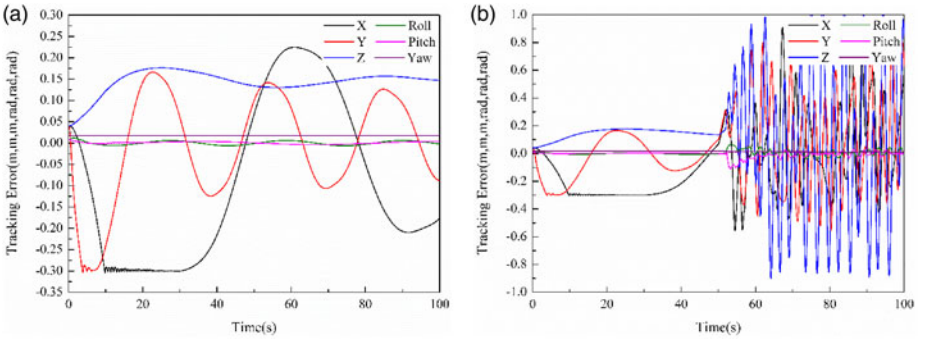

Figure 6. Comparative simulation results for the figure of eight curve shape trajectory.

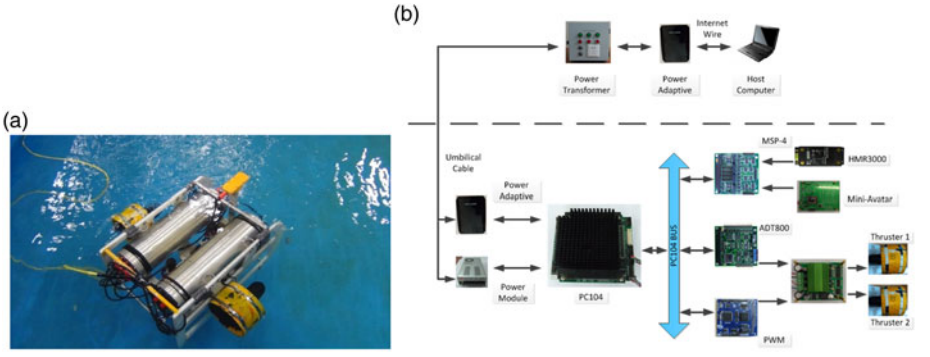

Figure 7. *Beaver 2* AUV and its hardware architecture.

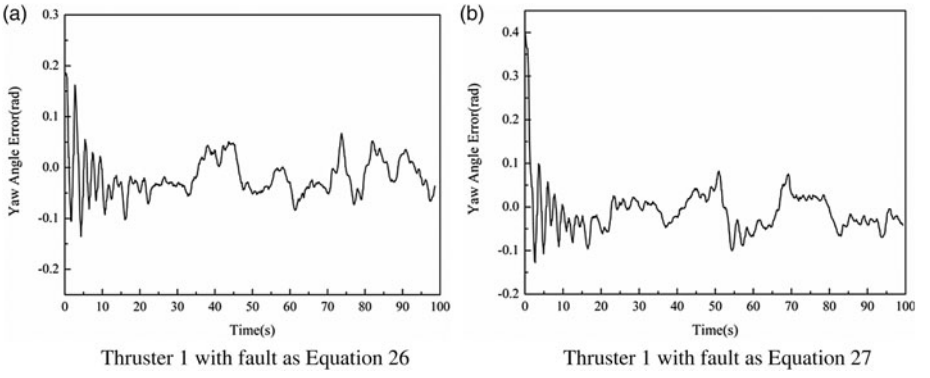

Figure 8. Experiments results for Yaw Angle 1.

https://doi.org/10.1017/S0373463316000370 Published online by Cambridge University Press

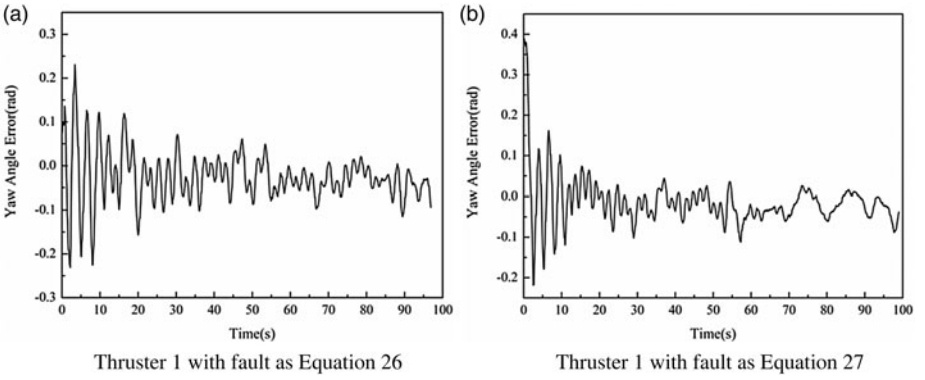

Figure 9. Experiments results for Yaw Angle 2.

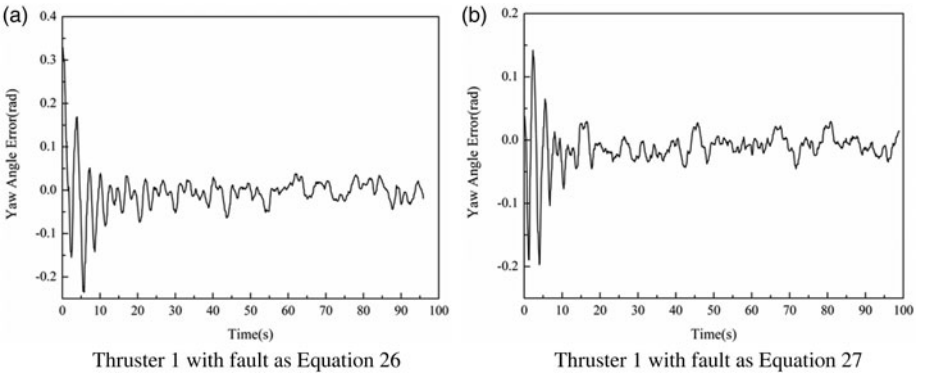

Figure 10. Experiments results for Yaw Angle 1 with another desired region.

8 and 9, although the tracking errors are outside of the desired region in the initial period, it reached the desired region after about 10 seconds based on the developed region tracking controller.

In addition, similar to Section 5.1, another desired region is used when tracking the first desired yaw angle, in the experiments with the above two kinds of different thruster faults, respectively. The new desired region: $\varepsilon_1 = 0{\cdot}05$, and the other parameters are not changed.

Figure 10 describes the experiments results for the two tracking cases. It can be seen from Figure 10 that the tracking error could reach the new desired region, no matter what kind of thruster fault occurs during the mission.

6. CONCLUSIONS. Adaptive region tracking fault tolerant control method is proposed for AUV while taking modelling uncertainty, ocean current disturbance, unknown thruster fault and thruster amplitude and rate saturation constraints into account simultaneously. The developed method is based on the backstepping technique. Information about thruster fault and ocean current disturbance is not required.

https://doi.org/10.1017/S0373463316000370 Published online by Cambridge University Press

Region tracking is achieved by constructing a continuous and piecewise Lyapunov function. Based on Barbalat's lemma, it demonstrates that the tracking errors could reach the designed region. Thruster amplitude and rate saturation constraints are transformed to a single constraint, and it is dealt with by locally modifying the desired trajectory. Simulation and pool experiments results illustrate the effectiveness of the proposed method.

ACKNOWLEDGMENTS

This work is supported by the National Natural Science Foundation of China (51279040) and Basic Research Program of Ministry of Industry and Information Technology of People's Republic of China (B2420133003).

REFERENCES

Aghaei, S., Sheikholeslam, F., Farina, M. and Scattolini, R. (2013). An MPC-based reference governor approach for offset-free control of constrained linear systems. *International Journal Of Control*, **86**, 1534–1539.

Ataei, M. and Yousefi-Koma, A. (2015). Three-dimensional optimal path planning for waypoint guidance of an autonomous underwater vehicle. *Robotics And Autonomous Systems*, **67**, 23–32.

Bessa, W.M., Dutra, M.S. and Kreuzer, E. (2010). An adaptive fuzzy sliding mode controller for remotely operated underwater vehicles. *Robotics And Autonomous Systems*, **58**, 16–26.

Bing, S., Daqi, Z. and Yang, S.X. (2014). A Bioinspired Filtered Backstepping Tracking Control of 7000-m Manned Submarine Vehicle. *Industrial Electronics, IEEE Transactions on*, **61**, 3682–3693.

Boussaid, B., Aubrun, C., Jiang, J. and Abdelkrim, M.N. (2014). FTC approach with actuator saturation avoidance based on reference management. *International Journal Of Robust And Nonlinear Control*, **24**, 2724–2740.

Chamseddine, A., Join, C. and Theilliol, D. (2013). Trajectory planning/re-planning for satellite systems in rendezvous mission in the presence of actuator faults based on attainable efforts analysis. *International Journal Of Systems Science*, **46**, 690–701.

Chamseddine, A., Theilliol, D., Zhang, Y.M., Join, C. and Rabbath, C.A. (2015). Active fault-tolerant control system design with trajectory re-planning against actuator faults and saturation: Application to a quadrotor unmanned aerial vehicle. *International Journal Of Adaptive Control And Signal Processing*, **29**, 1–23.

Chu, Z., Zhu, D. and Yang, S.X. (2016). Observer-Based Adaptive Neural Network Trajectory Tracking Control for Remotely Operated Vehicle. *IEEE Transactions on Neural Networks and Learning Systems*, PP, 1–13.

Fossen, T.I. (2011). *Handbook of marine craft hydrodynamics and motion control*. John Wiley & Sons.

Fossen, T.I., Pettersen, K.Y. and Galeazzi, R. (2015). Line-of-Sight Path Following for Dubins Paths With Adaptive Sideslip Compensation of Drift Forces. *Ieee Transactions On Control Systems Technology*, **23**, 820–827.

Gel'fand, I.M. and Shilov, G.E. (1964). *Generalized Fuctions*. Academic Press Inc.

Hu, Q., Xiao, B. and Friswell, M.I. (2011). Robust fault-tolerant control for spacecraft attitude stabilisation subject to input saturation. *Control Theory & Applications, IET*, **5**, 271–282.

Ismail, Z.H. and Dunnigan, M.W. (2011). Tracking control scheme for an underwater vehicle-manipulator system with single and multiple sub-regions and sub-task objectives. *IET Control Theory & Applications*, **5**, 721–735.

Ismail, Z.H., Faudzi, A.A. and Dunnigan, A.W. (2014). Fault-Tolerant Region-Based Control of an Underwater Vehicle with Kinematically Redundant Thrusters. *Mathematical Problems In Engineering*, 2014, 1–12.

Jiang, J. and Yu, X. (2012). Fault-tolerant control systems: A comparative study between active and passive approaches. *Annual Reviews in Control*, **36**, 60–72.

Johansen, T.A. and Fossen, T.I. (2013). Control allocation—A survey. *Automatica*, **49**, 1087–1103.

Koofigar, H.R. (2014). Robust Adaptive Motion Control with Environmental Disturbance Rejection for Perturbed Underwater Vehicles. *Journal of Marine Science and Technology-Taiwan*, **22**, 455–462.
Lekkas, A.M. and Fossen, T.I. (2014). Integral LOS Path Following for Curved Paths Based on a Monotone Cubic Hermite Spline Parametrization. *Ieee Transactions On Control Systems Technology*, **22**, 2287–2301.
Leonessa, A., Haddad, W.M., Hayakawa, T. and Morel, Y. (2009). Adaptive control for nonlinear uncertain systems with actuator amplitude and rate saturation constraints. *International Journal Of Adaptive Control And Signal Processing*, **23**, 73–96.
Li, X., Hou, S.P. and Cheah, C.C. (2010). Adaptive region tracking control for autonomous underwater vehicle. *Proceedings of the Control Automation Robotics & Vision (ICARCV), 2010 11th International Conference on*, Singapore.
Lombaerts, T., Looye, G., Chu, Q. and Mulder, J. (2012). Design and simulation of fault tolerant flight control based on a physical approach. *Aerospace Science And Technology*, **23**, 151–171.
Morishita, H.M. and Souza, C.E.S. (2014). Modified observer backstepping controller for a dynamic positioning system. *Control Engineering Practice*, **33**, 105–114.
Mukherjee, K., Kat, I.N. and Bhatt, R.K.P. (2015). Region tracking based control of an autonomous underwater vehicle with input delay. *Ocean Engineering*, **99**, 107–114.
Omerdic, E. and Roberts, G. (2004). Thruster fault diagnosis and accommodation for open-frame underwater vehicles. *Control Engineering Practice*, **12**, 1575–1598.
Podder, T.K. and Sarkar, N. (2001). Fault-tolerant control of an autonomous underwater vehicle under thruster redundancy. *Robotics And Autonomous Systems*, **34**, 39–52.
Seok Park, B. (2014). Neural Network-Based Tracking Control of Underactuated Autonomous Underwater Vehicles With Model Uncertainties. *Journal of Dynamic Systems, Measurement, and Control*, **137**, 021004.
Simplício, P., Pavel, M., Van Kampen, E. and Chu, Q. (2013). An acceleration measurements-based approach for helicopter nonlinear flight control using Incremental Nonlinear Dynamic Inversion. *Control Engineering Practice*, **21**, 1065–1077.
Slotine, J.J.E. and Li, W. (1991). *Applied Nonlinear Control*. Prentice Hall.
Soylu, S., Buckham, B.J. and Podhorodeski, R.P. (2008). A chattering-free sliding-mode controller for underwater vehicles with fault-tolerant infinity-norm thrust allocation. *Ocean Engineering*, **35**, 1647–1659.
Sun, B., Zhu, D. and Yang, S.X. (2016). A Novel Tracking Controller for Autonomous Underwater Vehicles with Thruster Fault Accommodation. *The Journal of Navigation*, **69**, 593–612.
Wang, T., Xie, W. and Zhang, Y. (2012). Sliding mode fault tolerant control dealing with modeling uncertainties and actuator faults. *Isa Transactions*, **51**, 386–392.
Wu, J., Li, J. and Chen, W. (2014). Semi-globally/globally stable adaptive NN backstepping control for uncertain MIMO systems with tracking accuracy known a priori. *Journal of the Franklin Institute*, **351**, 5274–5309.
You, S.S., Lim, T.W. and Jeong, S.K. (2010). General path-following manoeuvres for an underwater vehicle using robust control synthesis. *Proceedings of the Institution of Mechanical Engineers Part I-Journal of Systems and Control Engineering*, **224**, 960–969.
Zhang, M. and Chu, Z. (2014). Adaptive Region Tracking Control for Autonomous Underwater Vehicle. *Journal of Mechanical Engineering*, **50**, 50–57.
Zhang, M., Liu, X., Yin, B. and Liu, W. (2015). Adaptive terminal sliding mode based thruster fault tolerant control for underwater vehicle in time-varying ocean currents. *Journal of the Franklin Institute*, **352**, 4935–4961.

APPENDIX A. PROOF OF THEOREM 1

Define estimation error

$$\tilde{\rho}_i = \rho_i - \hat{\rho}_i \tag{A1}$$

Choose the following Lyapunov function

$$V_3 = V_2 + \frac{1-L}{2}\tilde{\rho}_0{}^T\Gamma_0\tilde{\rho}_0 + \frac{1-L}{2}\tilde{\rho}_1^T\Gamma_1\tilde{\rho}_1 + \frac{1-L}{2}\tilde{\rho}_2^T\Gamma_2\tilde{\rho}_2 + \frac{1-L}{2}\tilde{\rho}_3^T\Gamma_3\tilde{\rho}_3 \tag{A2}$$

https://doi.org/10.1017/S0373463316000370 Published online by Cambridge University Press

The derivative of Equation (A2) is

$$\dot{V}_3 = \dot{V}_2 - (1-L)\tilde{\rho}_0^T\Gamma_0\dot{\hat{\rho}}_0 - (1-L)\tilde{\rho}_1^T\Gamma_1\dot{\hat{\rho}}_1 - (1-L)\tilde{\rho}_2^T\Gamma_2\dot{\hat{\rho}}_2 - (1-L)\tilde{\rho}_3^T\Gamma_3\dot{\hat{\rho}}_3 \quad \text{(A3)}$$

Substituting Control law Equation (19) and adaptive law Equation (20) into Equation (A3), yielding

$$\begin{aligned}
\dot{V}_3 \le{}& \Sigma(-g_1(kP_{3,\varepsilon_1}(z_1) + P_{2,\varepsilon_1}(z_1))^2 - g_2(kP_{2,\varepsilon_2}(z_2) + P_{1,\varepsilon_2}(z_2))P_{1,\varepsilon_2}(z_2) + W \\
&+ (kP_{2,\varepsilon_2}(z_2) + P_{1,\varepsilon_2}(z_2))(-(1-L)(\hat{\rho}_0 + \hat{\rho}_1\|\dot{\eta}\| + \hat{\rho}_2\|\dot{\eta}\|^2) + H) \\
&- (kP_{2,\varepsilon_2}(z_2) + P_{1,\varepsilon_2}(z_2))(\hat{M}_\eta^{-1}(1-L)\hat{\rho}_3 - [L,L,L]^T)\phi \\
&- (1-L)\tilde{\rho}_0^T(kP_{2,\varepsilon_2}(z_2) + P_{1,\varepsilon 2}(z_2)) - (1-L)\tilde{\rho}_1^T(kP_{2,\varepsilon_2}(z_2) \\
&+ P_{1,\varepsilon_2}(z_2))\|\dot{\eta}\| - (1-L)\tilde{\rho}_2^T(kP_{2,\varepsilon_2}(z_2) + P_{1,\varepsilon_2}(z_2))\|\dot{\eta}\|^2 \\
&- (1-L)\tilde{\rho}_3^T\hat{M}_\eta^{-1}(kP_{2,\varepsilon_2}(z_2) + P_{1,\varepsilon_2}(z_2))\phi)
\end{aligned} \quad \text{(A4)}$$

where, $\phi = \left\|[(\hat{C}_{RB\eta}\dot{\eta} + \hat{C}_{A\eta}\dot{\eta} + \hat{D}_\eta\dot{\eta} + \hat{g}_\eta) + \hat{M}_\eta\dot{\alpha}_1 - (g_2+1)\hat{M}_\eta P_{1,\varepsilon_2}(z_2)\mathrm{sgn}_{\varepsilon_2}(z_2)]\right\|$;

$$\begin{aligned}
W = \Sigma(&-\frac{1}{4}(kP_{3,\varepsilon_1}(z_1) + P_{2,\varepsilon_1}(z_1))^2 + (kP_{3,\varepsilon_1}(z_1) + P_{2,\varepsilon_1}(z_1))(|z_2| - (\varepsilon_2 + \sigma)) \\
&- (kP_{2,\varepsilon_2}(z_2) + P_{1,\varepsilon_2}(z_2))P_{1,\varepsilon_2}(z_2)).
\end{aligned}$$

When $|z_2| < (\varepsilon_2 + \sigma)$, it is straightforward that $W < 0$. And when $|z_2| \ge (\varepsilon_2 + \sigma)$, integrating with Young's Inequality, we can derive the following inequality

$$\begin{aligned}
W &\le \Sigma((|z_2| - (\varepsilon_2 + \sigma))^2 - (kP_{2,\varepsilon_2}(z_2) + P_{1,\varepsilon_2}(z_2))P_{1,\varepsilon_2}(z_2)) \\
&\le \Sigma((|z_2| - (\varepsilon_2 + \sigma))^2 - P_{\varepsilon 2,1}(z_2)^2 = (|z_2| - (\varepsilon_2 + \sigma))^2 \\
&\quad - \exp(k(|z_2| - \varepsilon_2)) \times (|z_2| - \varepsilon_2)^2) \\
&\le \Sigma(|z_2| - (\varepsilon_2 + \sigma))^2 - \Sigma(|z_2| - \varepsilon_2)^2 < 0
\end{aligned} \quad \text{(A5)}$$

Therefore, according to Equations (5) and (8), Inequality (A4) can be presented

$$\begin{aligned}
&\dot{V}_3 \le \Sigma(-g_1(kP_{3,\varepsilon_1}(z_1) + P_{2,\varepsilon_1}(z_1))^2 - g_2(kP_{2,\varepsilon_2}(z_2) + P_{1,\varepsilon_2}(z_2))P_{1,\varepsilon_2}(z_2)) \\
&\le \Sigma(-g_1(kP_{3,\varepsilon_1}(z_1) + P_{2,\varepsilon_1}(z_1))^2)
\end{aligned} \quad \text{(A6)}$$

Since Lyapunov function $V_3 > 0$ and $\dot{V}_3 \le 0$, V_3 is bounded. So z_1, z_2 and $\tilde{\rho}_i$, $i = 0,1,2,3$ are bounded. And since the reference states η_r $\dot{\eta}_r$ and $\ddot{\eta}_r$ are bounded, the virtual variable α is bounded from Equation (15).

Let $\Delta = \Sigma(g_1(kP_{3,\varepsilon_1}(z_1) + P_{2,\varepsilon_1}(z_1))^2)$. Integrating Inequality Equation (A6) at the interval of [0, t], we have $\int_0^t \Delta(\vartheta)d\vartheta \le V_3(0)$, which means $\int_0^t \Delta(\vartheta)d\vartheta$ has a finite limit as $t \to \infty$. According to Equation (3), we can see that Δ is differentiable, and the derivative of Δ is a function of $\dot{z}_1$. From Equation (10), the boundedness of $\dot{z}_1$ can be ensured. So we can prove that the derivative of Δ is bounded. Thus, we conclude that Δ is uniformly continuous.

Consequently, according to the facts that $\int_0^t \Delta(\vartheta)d\vartheta$ has a finite limit as $t \to \infty$ and Δ is uniformly continuous, it can be concluded that Δ equals to zero, as $t \to \infty$ based on Barbalat's lemma, which means $z_1 \le \varepsilon_1$ as $t \to \infty$. This completes the proof.

https://doi.org/10.1017/S0373463316000370 Published online by Cambridge University Press

APPENDIX B. PROOF OF THEOREM 2

Statement (i) can be directly proved according to Appendix A.

In order to prove statement (ii), substituting Equations (23) and (24) into Equation (19), we can derive

$$\begin{aligned} u = {} & B^{+}J^{T}[(\hat{C}_{RB\eta}\dot{\eta} + \hat{C}_{A\eta}\dot{\eta} + \hat{D}_{\eta}\dot{\eta} + \hat{g}_{\eta}) \\ & + \hat{M}_{\eta}\Big(\frac{df(z_1)}{dt} - \omega_n^2\eta_R - 2\omega_n\xi\dot{\eta}_R \\ & + \omega_n^2(\eta_d + (\omega_n^2 J^T\hat{M}_{\eta})^{-1}Bu^*(\delta(u^*) - 1))\Big) \\ & - (c_2 + 1)\hat{M}_{\eta}P_{\varepsilon 2,1}(z_2)\mathrm{sgn}_{\varepsilon 2}(z_2)] + u_1 + u_2 \\ = {} & u^* + u^*(\delta(u^*) - 1) \\ = {} & u^*\delta(u^*) \end{aligned} \tag{B1}$$

From the property of $\delta(u^*)$ and Equation (B1), it is implied that the control outputs after modifying the desired trajectory as Equation (24) are guaranteed to satisfy the thruster amplitude and rate saturation constraints as Equation (22). This completes the proof.

https://doi.org/10.1017/S0373463316000370 Published online by Cambridge University Press